iScience

CellPress
OPEN ACCESS

Article

Effect of ion migration on lead halide perovskite on visible light communication system

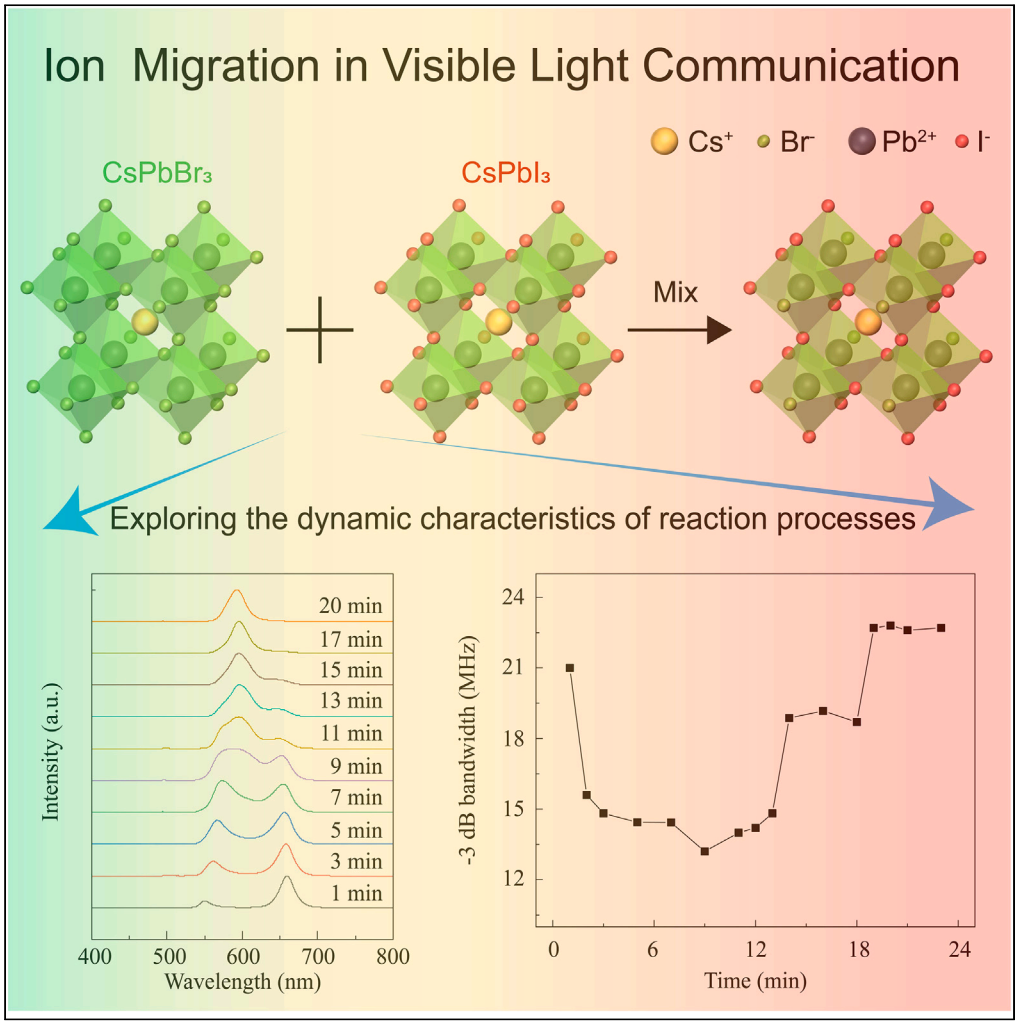

Haocheng Tang, Yichi Zhong, Jingzhou Li, ..., Hongyu Yang, Hongxing Dong, Long Zhang

lijingzhou@ucas.ac.cn (J.L.)
hongxingd@siom.ac.cn (H.D.)

Highlights

The ion migration process is realized by mixing $CsPbBr_3$ and $CsPbI_3$ quantum dots

PL lifetime variations of perovskite LED device during ion migration are measured

The modulation scheme of the perovskite LED device achieved a data rate of 90 Mbps

Tang et al., iScience *26*, 108173
November 17, 2023
https://doi.org/10.1016/j.isci.2023.108173

iScience

CellPress
OPEN ACCESS

Article

Effect of ion migration on lead halide perovskite on visible light communication system

Haocheng Tang,[1,2,3,5] Yichi Zhong,[2,4,5] Jingzhou Li,[2,3,6,*] Luyang Hou,[1,2,3] Xizhe Liang,[1,2,3] Jiahao Zhang,[1,2,3] Hongyu Yang,[2,3] Hongxing Dong,[1,2,3,*] and Long Zhang[1,2]

SUMMARY

Benefiting from the high modulation bandwidth (BW), low energy consumption and excellent optical performance, lead halide perovskite has attracted wide attention in visible light communication (VLC). However, the ion migration which results in mobile point defects in perovskite structures is recognized as a crucial key factor inducing the performance degradation. Here, the influence of ion migration in perovskite devices on the performance of VLC was systematically studied. The ion migration process is realized by mixing $CsPbBr_3$ and $CsPbI_3$ quantum dots, during which, the performance of the VLC system is reduced, but it can return to its initial state after stabilization. The on-off keying (OOK) modulation scheme of the perovskite light-emitting diode (LED) device was carried out, achieving a data rate of 90 Mbps.

INTRODUCTION

Visible light communication (VLC), which modulates the visible light spectrum to transfer data transmission, has become popular in fulfilling the growing demand for wireless data communication,[1,2] resulted from the high transmission rate, low energy consumption and strong anti-electromagnetic interference capability. Moreover, the VLC can provide unauthorized and secure bandwidth (BW) of up to hundreds of terahertz in visible light bands in the range of 380 nm–790 nm to alleviate congestion BW in RF radio frequency networks.[3–5] These advantages make VLC an indispensable wireless communication mode in the future intelligent era of 6G ultra-high speed ubiquitous optical network. Meanwhile, the VLC system can be compatible with the illumination function to realize the integration of communication and illumination. As the commonly light signal transmitters in VLC systems, the white light-emitting diodes (LEDs), which are typically created by combining an ultraviolet (UV) LED chip with different phosphors, are one of the key factors of VLC system performance.[6–9] However, a restricted factor of the VLC application is the low BW owing to relatively long photoluminescence (PL) lifetime of conventional phosphors in the white LED. Currently, the BW of the LED is about 3–12 MHz based on YAG- and nitride-rare earth phosphors, and is about 40–200 MHz based on organic materials and Cd-nanocrystals.[9–12] It is noteworthy that these results are obtained together with the UV LED chips. According to the rule of the device BW $\leq 1/2\pi\tau$ (τ is the PL lifetime of the materials),[13] the device BW will be smaller (usually <10 MHz) if the harmful UV light is filtered out in the actual application.[14,15]

Perovskite materials have received substantial attention due to their high photoluminescence quantum yield (PLQY), tunable emission across the entire visible region, and narrow emission linewidth below 20 nm.[16–18] High PLQY is one of the crucial features of QDs and a significant reason for their application in VLC, in which the photodetection efficiency of the receiver directly affects the receiving sensitivity of the system. Perovskite materials with high PLQY can emit light signals effectively, enhancing the receiver's sensitivity and stability.[19,20] Furthermore, the PL lifetime of the perovskite quantum dots (QDs) can be up to subnanosecond,[21,22] which means that high BW can be obtained in a perovskite-based VLC system.[23,24] The white LED containing perovskite materials and UV chip was proposed to serve as light source in VLC system by Bakr et al.,[25] in which a maximum −3 dB BW up to 500 MHz is obtained.[26] Moreover, the data rate modulation mode for the VLC system based on perovskites, such as on-off keying (OOK) and orthogonal frequency division multiplexing (OFDM), are also researched.[27] Although those VLC systems have shown excellent communication performance, there is a comprehensive problem of ion migration in perovskite white LED devices,[28–30] which has been widely acknowledged as the key factor causing the optical performance degradation of the perovskite LED device. So far, the influence of ion migration on VLC systems in perovskite LED devices is still blank.

In this work, we focus on the light communication performance of the mixed $CsPbBr_3$ and $CsPbI_3$ perovskite LED device in VLC system. Based on the effect of ion migration, a series of wavelengths ranging from green to red can be obtained. With the measurement of the BW and data transmission rate variation during the ion migration reaction, we demonstrated that the optical performance of VLC system would be

[1]Shanghai Institute of Optics and Fine Mechanic, Chinese Academy of Sciences, Shanghai 201800, China
[2]Hangzhou Institute for Advanced Study, University of Chinese Academy of Science, Hangzhou 310024, China
[3]University of Chinese Academy of Sciences, Beijing 100049, China
[4]Department of Physics, College of Mathematics and Physics, Chengdu University of Technology, Chengdu 610059, China
[5]These authors contributed equally
[6]Lead contact
*Correspondence: lijingzhou@ucas.ac.cn (J.L.), hongxingd@siom.ac.cn (H.D.)
https://doi.org/10.1016/j.isci.2023.108173

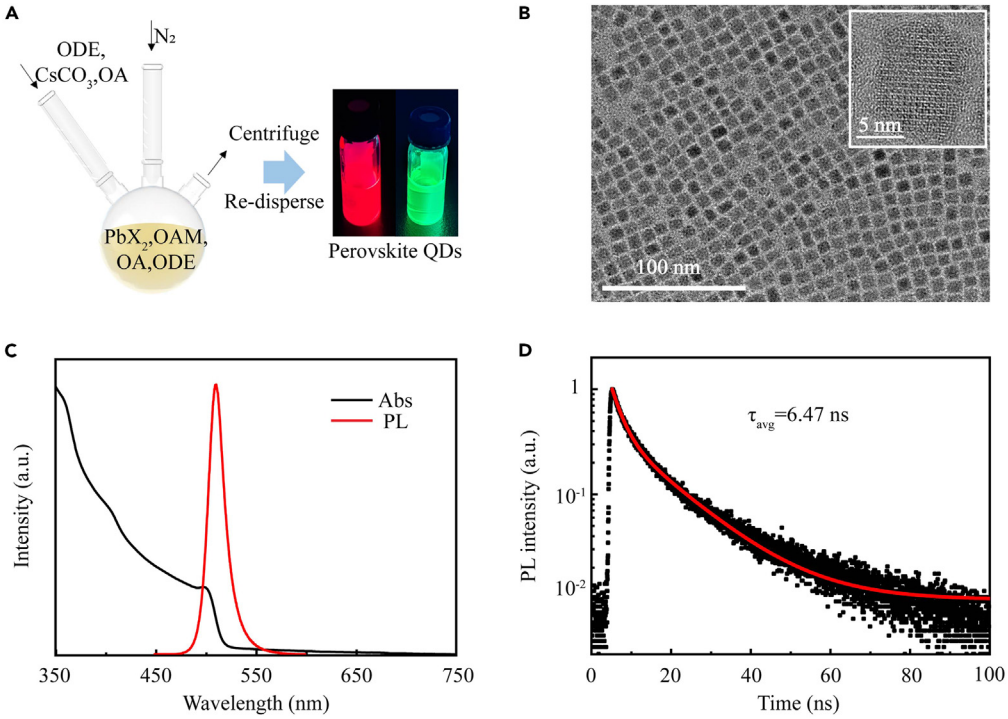

Figure 1. Fabrication process and optical characterization of the perovskite QDs

(A) Schematic illustrations for the synthesis processes of QDs.

(B) TEM images of the $CsPbBr_3$ QDs. Inset: HRTEM image.

(C) PL spectrum with emission peak at 515 nm and the absorption spectrum of the $CsPbBr_3$ QDs.

(D) PL decay curves and biexponential fitting curve of the $CsPbBr_3$ QDs with a fast and a slow lifetime of τ_1 ~2.54 ns (~62.6%) and τ_2 ~13.05 ns (~37.4%), respectively.

degraded when ion migration occurs and can return to excellent performance when the system can be re-stabilized. With the UV light been filtered out, a −3 dB BW as 50 MHz was obtained during the ion migration, which reached 80 MHz when the system returned to stability.

RESULTS AND DISCUSSION

The as-prepared $CsPbBr_3$ and $CsPbI_3$ QDs according to the previously reported hot-injection method with minor modifications are shown in Figure 1A. As shown in Figure 1B, transmission electron microscopy (TEM) reveals that the $CsPbBr_3$ QDs are regular cubic. The excellent crystallinity and few defects can be clearly seen through high-resolution TEM (HRTEM) in the inset of Figure 1B. These excellent QD structures ensure efficient PLQY of up to 90%. The corresponding statistical plot of crystalline grain distribution is shown in Figure S1A, which shows the average size of 11 nm with a deviation of ± 2 nm. Since the size distribution can affect the optical and electrical properties of QDs due to the quantum size effect,[31] QDs with uniform size can manifest as a perfect PL signal with narrower full width at half maximum (FWHM), which is of great importance for the output signal amplitude flatness of the VLC system. Figure 1C shows the absorption (black) and PL (red) spectrum of $CsPbBr_3$ QDs. The $CsPbBr_3$ QDs have a broad absorption band and a sharp PL emission at 515 nm with a narrow FWHM of 19 nm. Figure 1D shows the PL dynamic of the $CsPbBr_3$ QDs. The decay curve was fitted with the biexponential functions given in the Equation 1.[32]

$$A(t) = A_1 \exp\left(\frac{-t}{\tau_1}\right) + A_2 \exp\left(\frac{-t}{\tau_2}\right) \quad \text{(Equation 1)}$$

Through fitting, a fast component and a slow lifetime component with τ_1 ~2.54 ns and τ_2 ~13.05 ns, respectively, are obtained. The amplitude values A_1 ~4.74, and A_2 ~0.55 are considered the weighing factors. The average decay lifetime $\tau_{avg.}$ is calculated Equation 2.[32]

$$\tau avg. = \frac{A_1\tau_1^2 + A2\tau_2^2}{A_1\tau_1 + A_2\tau_2} \quad \text{(Equation 2)}$$

The $\tau_{avg.}$~6.47 ns of $CsPbBr_3$ QDs is much shorter than that of most fluorescent dyes,[33–35] which implies that the $CsPbBr_3$ QDs are ideal high-speed luminescent material. In addition, the characterization analyses of $CsPbI_3$ QDs in Figures S1B–S1D show that $CsPbI_3$ QDs exhibit a PL spectrum peak at 682 nm. This makes $CsPbI_3$ QDs suitable as a material for studying the communication performance of ion migration in perovskite LED system through anion exchange.[36]

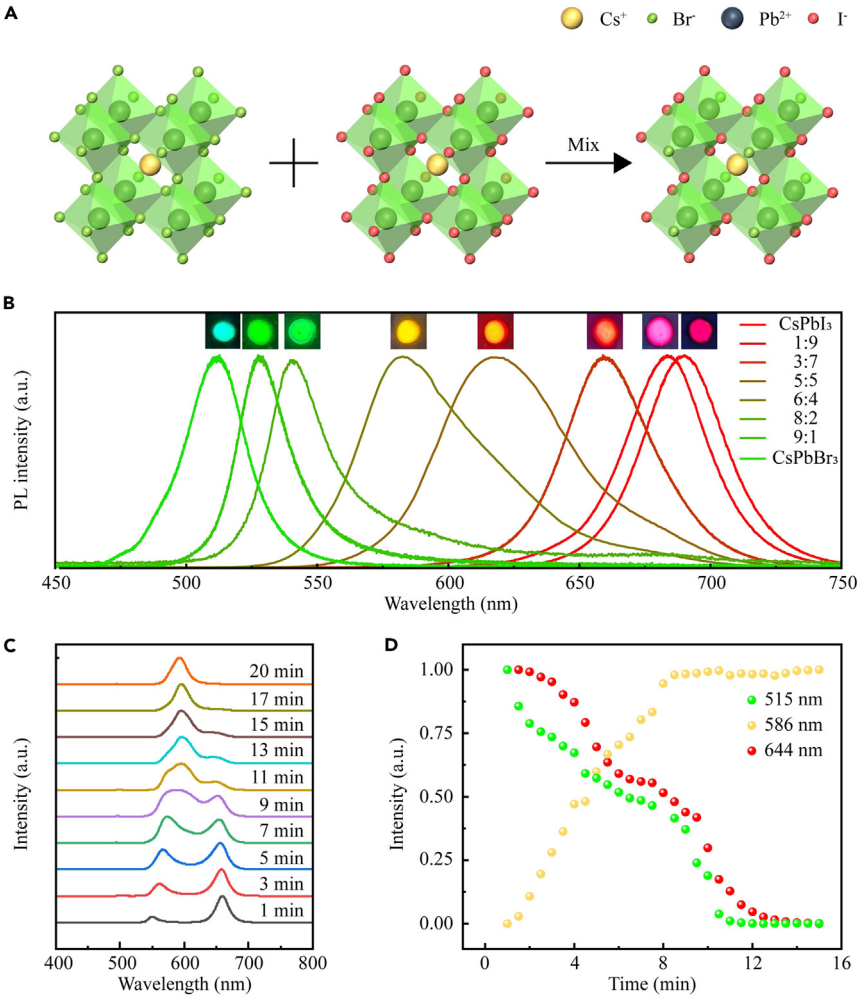

Figure 2. Ion migration process of $CsPbBr_3$ and $CsPbI_3$ QDs

(A) Schematic diagram of ion migration.

(B) PL spectra and photographs of the $CsPbBr_xI_{3-x}$ QDs prepared by anion exchange with $CsPbBr_3$ and $CsPbI_3$ QDs in different proportions.

(C) PL spectra changes of the reaction solution (Br: I = 6: 4) during the 15 min anion exchange reaction.

(D) PL intensity changes at 515 nm, 586 nm, and 644 nm during the anion exchange reaction.

The ion migration process is mainly dominated by anion exchange between $CsPbBr_3$ and $CsPbI_3$ QDs, which is vividly sketched by Figure 2A. $CsPbX_3$ QDs have excess halide ions on the surface. Being more ionic in nature, passivating ligands, oleylammonium ions and anions can quickly come off as oleylammonium halide (OLAmX) from the perovskite nanocrystal surface, the interparticle mixing of $CsPbBr_3$ and $CsPbI_3$ nanocrystals lead to an anion exchange within the nanocrystals through the OLAmX.[37] The reaction produces $CsPbBr_xI_{3-x}$ QDs, where x depends on the molar ratios of the two raw materials. Figure 2B shows the normalized PL spectra curve of $CsPbBr_xI_{3-x}$ films after the exchange, in which the proportion of $CsPbI_3$ QDs molar ratio increased from 0% to 100% with the PL emission shifted from 515 nm to 682 nm. The insets at top of each curve correspond to the photographs of the fluorescent films, which demonstrate neglectable PL degradation after anion exchange. To illustrate the anion exchange reaction process, the PL spectra were continuously recorded for 20 min, as shown in Figure 2C. Two original PL emission peaks at 515 nm ($CsPbBr_3$) and 682 nm ($CsPbI_3$) were observed at the beginning of the reaction and gradually decreased in the first few minutes. Over time, both the $CsPbBr_3$ side peak and the $CsPbI_3$ side peak gradually shift toward longer and shorter wavelengths respectively, accompanied by a decrease in their corresponding intensities. Meanwhile a new peak emerges while the two original peaks intensity decreases and eventually, all the peaks merge to a single peak at the end of the reaction. The reduction of red and green peaks and the formation of new peaks correspond to the interparticle mixing reaction of $CsPbBr_3$ and $CsPbI_3$ QDs. As further illustrated in Figure 2D, with the reaction prolonging from 1 min to 16 min, the PL intensity of the wavelength 515 nm and 682 nm decreased rapidly and almost extinction, while the PL intensity at 586 nm quickly increased to the top. Anion exchange between QDs took up to several minutes to reach a steady state most likely because the halides ions had to cruise in the solvent.[36] The evolution of these PL spectra reveals that the nature of anion exchange is different from the traditional anion exchange process in introducing additional anions, proving that this method is convenient for making fluorescent films with different colors.

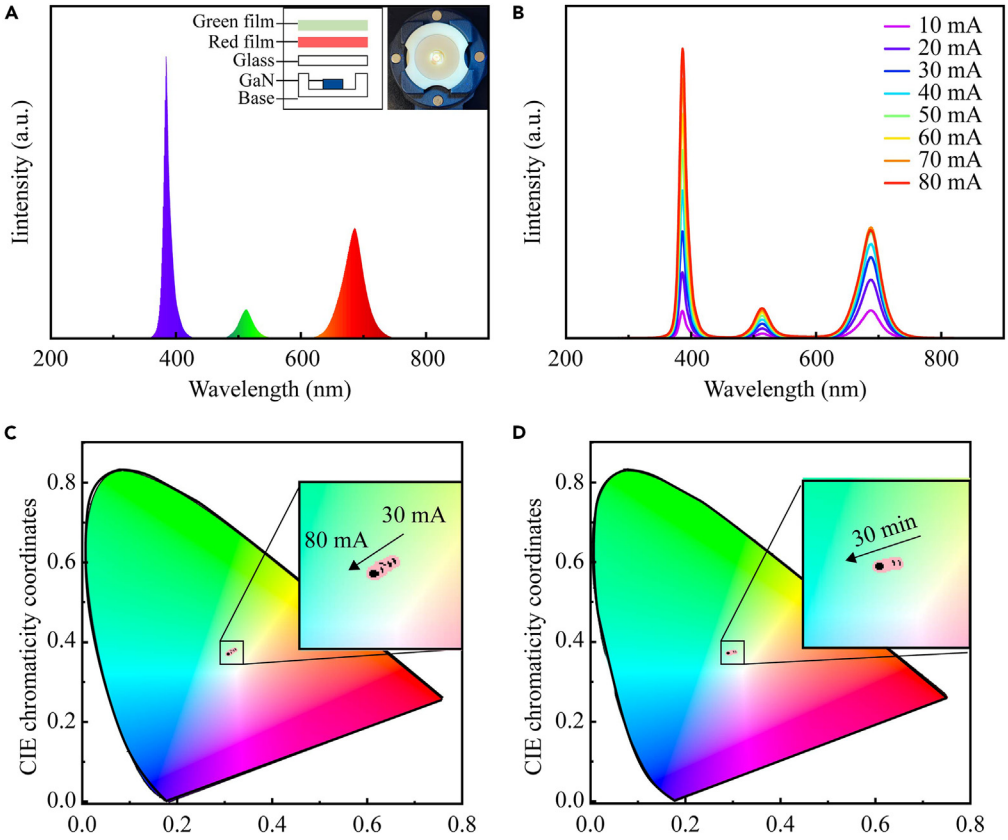

Figure 3. The light performance of the LED device based on perovskite QDs

(A) Emission spectra of laminated fluorescent film driven at 80 mA, inset: Schematic diagram and photograph of the perovskite LED device.

(B) Emission spectra of the laminated fluorescent film under different forward currents.

(C) CIE chromaticity coordinates of laminated LED.

(D) CIE chromaticity coordinates of the color shift of the laminated LED during the continuous operation for 30 min.

The perovskite LED device in the VLC system is shown in the inset at top-right of Figure 3A, which consists of different perovskite QDs films and an LED chip that emits light at 385 nm with FWHM of 15 nm. The optical performance of the LED device was performed using an integrating sphere by supplying an alternating current to a direct-current bias tee which was used to drive the LED. In order to prevent the films from being destroyed by direct contact with a high-temperature chip that operates for a long time, green and red films were placed on a thin piece of glass above the chip. In addition, the green films are placed at top to avoid the light emitted by which being entirely absorbed by the red films.

Figure 3A shows the emission spectrum of the laminated LED using a red mixture film (Br: I = 1: 9) and a green mixture film (Br: I = 9: 1) driving by 80 mA current at room temperature. Three peaks are observed for the chip (385 nm), green light (527 nm), and red light (672 nm), respectively, the emission spectra of these films with the drive current increased from 10 to 80 mA is shown in Figure 3B. By elevating the operating current, the emission light intensities of those films climb gradually with the PL emission peak barely changed. Further, the variation of the correlated color temperature (CCT) calculated chromatic coordinates of the laminated LEDs plotted in the CIE 1931 color space shown in Figure 3C, the chromatic coordinates (x, y) of which change from (0.3097, 0.3867) to (0.2957, 0.3765) with increasing the current from I = 30 to 80 mA, and the CCT changes from 6320.2 K to 6950.7 K. Figure 3D shows the CCT changes of these fluorescent films over 30 min through the CIE 1931 color space with the driving current at 50 mA. The chromatic coordinates (x, y) of the laminated LED change from (0.2964,0.3775) to (0.2826,0.3751) with the increase of the time and the CCT changes from 6912.5 K to 7552.6 K which clearly shows that QDs have good stability over a long period of time, therefore, the laminated LED device is very promising for the VLC system because the emission lights of the fluorescent films are stable when the driving current fluctuates, which indicates that the influence of QDs instability on the communication system can be ignored.

To investigate the effect of ion migration on communication performance based on perovskite materials, a VLC system was designed and set up as shown in Figure S2, which includes the arbitrary waveform generator (RIGOL DG70004), spatial optical path, avalanche photodiode (Thorlab APD210), and oscilloscope (RIGOL DS70504). A pseudorandom binary sequence data format was sent to the light source which emitted signal light through a series of planoconvex lenses, an objective lens with a focal length of 2 cm, and two filters (550 nm long

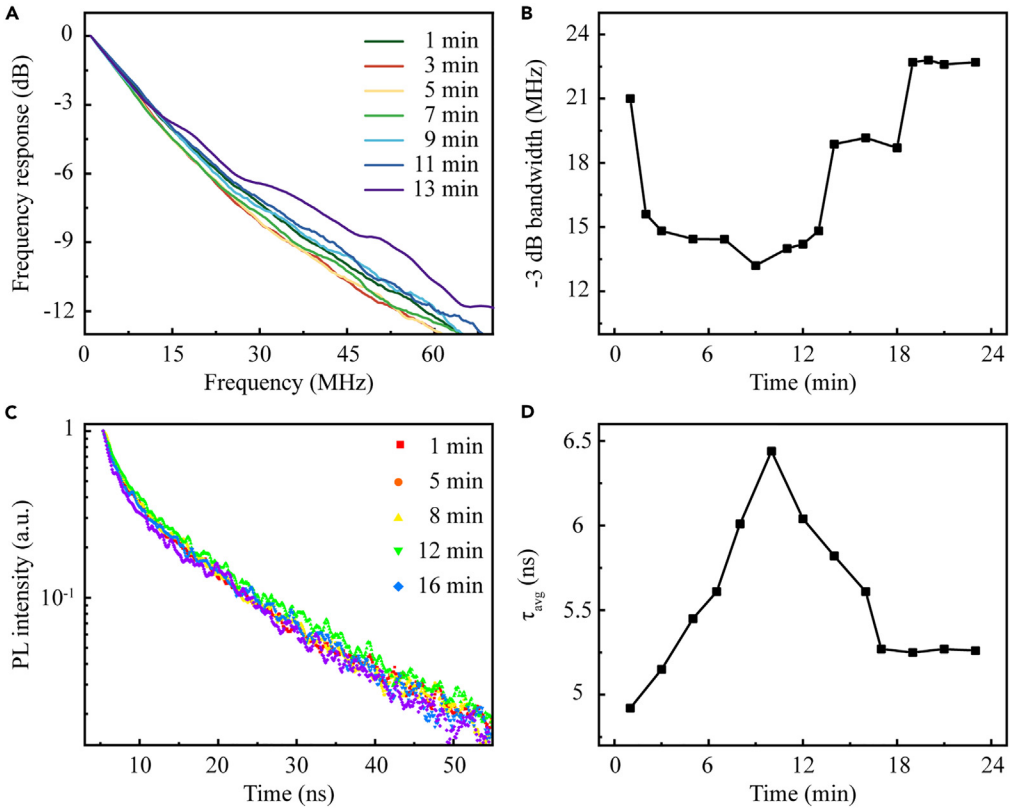

Figure 4. The optical communication performance of the perovskite QDs mixture

(A) Modulation BW of the mixture during the ion exchange.

(B) The maximum -3dB BW changes at the time from 1 min to 23 min.

(C) Time-resolved PL decays of the mixture during the ion exchange.

(D) The PL lifetime change at the time from 1 min to 23 min.

pass and 600 nm short pass) before entering the APD, so that the light of the parents QDs were filtered out to avoid their interference. The distance between the light source and the Si-based APD was approximately 40 cm. The frequency responses of the VLC system were measured from 1 MHz to 80 MHz using a network analyzer. Figure 4A shows the frequency response for the perovskite QDs mixture (Br: I = 5:5). The maximum −3 dB BW of the mixture was obtained to be 21 MHz in the beginning of the anion exchange reaction, which drastically dropped to 14 MHz but further increased over the next few minutes. The evolution of −3 dB BW was analyzed as shown in Figure 4B which indicates that the modulation BW curves of the mixture decreased when the QDs with different anions first exposed to each other and then flatten out after the ion exchange reaction finished. In addition, the time-resolved PL decays of two kinds of QDs during ion exchange was measured as shown in Figure 4C and their fitting results are summed in Figure 4D. The radiative lifetimes gradually and sequentially increase in the first few minutes then decrease and the $\tau_{avg.}$ of which reached a maximum in about 10 min after the reaction began and decreased consistently over the next several minutes, in which the climb and the diminution of the $\tau_{avg.}$ correspond to the variation tendency of the BW. The fast partition dynamics of halide ions between the QDs and the solution phase is responsible for the changes of PL lifetime and BW. As an essential factor in the VLC system, the PL lifetime of perovskite QDs has a binding impact on the modulation BW of the system,[37] thus the changes of −3 dB BW here imply that ion migration may have a ripple effect on the PL lifetime of QDs.

The communication performances are tested through the OOK modulation scheme[38–40] which is a unipolar nonreturn-to-zero code sequence to control the opening and closing of square wave carriers, with one amplitude set to 0 and the other amplitude set to non-0. Figure 5A shows the BER data during the anion exchange in which the ratio of parents QDs was the same as in Figure 2C. Since the reaction time could be affected by physical factors such as vibration and agitation, the intensity change of the middle PL peak was used as the abscissa. A data rate of 50 Mbps was given to the light source. The BER of the system gradually decreased with the increased of PL intensity at 586 nm, with most of the points closed to the forward error correction (FEC) limit of 3.8×10^{-3}. After the reaction was completed, the BER of the system reached 2×10^{-4}, which ensured the reliability of data transmission in the VLC system. Eye diagrams correspond to Figure 5A are shown in Figures S3A–S3C, which suggest that the perovskite QDs can transmit a data rate of more than 50 Mbps even during the anion exchange reaction. Therefore, the perovskite-based VLC system can maintain stable operation at high data rates even when ion migration occurs.

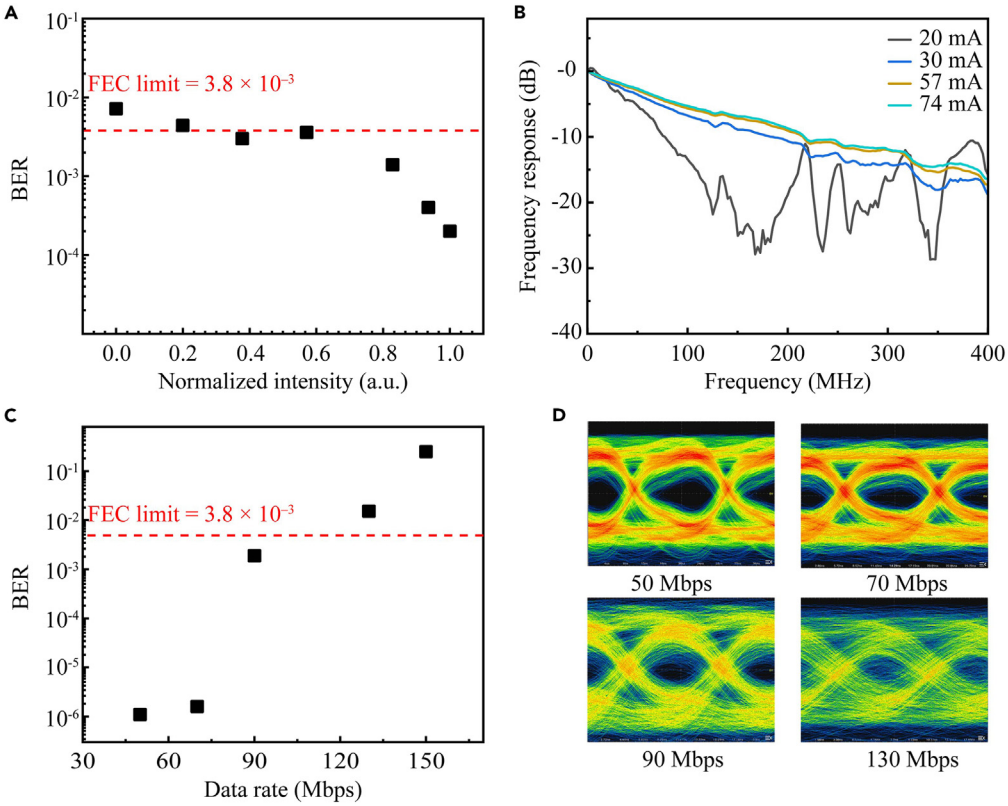

Figure 5. The optical communication performance of the perovskite LED device

(A) Bit error rate (BER) variation with the PL intensity of the mixture at 586 nm during the reaction.

(B) Modulation BW of laminated fluorescent films under different forward currents.

(C) BER of laminated fluorescent films under different data rates.

(D) The corresponding eye diagrams at different data rates.

Since the BW performance of the perovskite solution can be deteriorated by the effects existing in the solution such as reflection, refraction, and self-absorption phenomena, the frequency responses for the perovskite fluorescent film (Br: I = 5: 5) along the driving current increased were measured as shown in Figure 5B, which were feeble with the current below 30 mA, while reached about 80 MHz and showed slight fluctuation after the current reached 57 mA. This indicates that the system will show excellent stability when the driving current reaches normal level. Figure 5C shows the BERs at different data rates in free space at the light source injection current of 60 mA. The highest achievable data rate was recorded more than 90 Mbps, with a measured BER of 1.9×10^{-3}, below the FEC limit. The corresponding eye diagram with the data rate of 90 Mbps is shown in Figure 5D, the eye is open and clear. Figure 5D presents the eye diagrams of the system data rates of 50, 70, 90, and 130 Mbps, respectively. The eye diagrams with data rate below 70 Mbps are open and clear, which is attributed to the high BW of the fluorescent film.

Conclusions

This study investigated how the optical performance of the perovskite-based VLC system is affected by the ion migration. Green $CsPbBr_3$ and red $CsPbI_3$ QDs were synthesized first following the hot-injection method. By simply mixing these highly luminescent $CsPbBr_3$ and $CsPbI_3$ QDs with different molar ratios, stable and efficient luminescence with various emission peaks (from 515 to 682 nm) were obtained based on the effect of ion migration. Time-dependent PL studies revealed three different emission peaks during the evolution—a green side peak, a red side peak, and a new intermediate peak. Meanwhile, the BW were strictly tracked to probe the optical performance variation of the VLC system, during which the structure conversion of perovskite QDs can lead to a ripple effect on the system, which is attributed to the BW degradation. By employing the OOK modulation scheme, we verified that the VLC system based on the fluorescent films reached high modulation BW and transmitted signal steadily. These results will support the development of high stability VLC applications.

Limitations of the study

This research examines the dynamic process and communication behavior of lead halide perovskite ion exchange. The reaction is significantly influenced by external factors such as temperature and environmental conditions, therefore requiring a high level of measurement accuracy to reproduce consistent result.

STAR★METHODS

Detailed methods are provided in the online version of this paper and include the following:

- KEY RESOURCES TABLE
- RESOURCE AVAILABILITY
  - Lead contact
  - Materials availability
  - Data and code availability
- METHOD DETAILS
  - Preparation of $CsPbX_3$ (X = Br and I) perovskite QDs
  - Preparation of the fluorescent film

SUPPLEMENTAL INFORMATION

Supplemental information can be found online at https://doi.org/10.1016/j.isci.2023.108173.

ACKNOWLEDGMENTS

This work was supported by the National Natural Science Foundation of China (Grant No. 62205084), the National Natural Science Foundation of China (Grant No. 12104110), and the Zhejiang Province Public Welfare Technology Application Research Project (Grant No. LGN22F050002).

AUTHOR CONTRIBUTIONS

H.T. and Y.Z. fabricated the samples and conceived experiments. H.T., Y.Z., and L.H. carried out the scanning electron microscopic and TEM measurements. H.T., Y.Z., X.L., and J.Z. carried out the communication performances test. H.T., Y.Z., and H.Y. wrote the manuscript. J.L., H.D., and L.Z. supervised the research and led the project.

DECLARATION OF INTERESTS

The authors declare no competing interests.

Received: April 9, 2023
Revised: July 25, 2023
Accepted: October 8, 2023
Published: October 11, 2023

REFERENCES

1. Chi, N., and Chen, H. (2020). Progress and prospect of high-speed visible light communication. Guangdian Gongcheng/Opto-Electron. Eng. *47*, 1–12. https://doi.org/10.12086/oee.2020.190687.
2. Ali, A., Qasem, Z.A.H., Li, Y., Li, Q., and Fu, H.Y. (2022). All-inorganic liquid phase quantum dots and blue laser diode-based white-light source for simultaneous high-speed visible light communication and high-efficiency solid-state lighting. Opt Express *30*, 35112–35124. https://doi.org/10.1364/oe.469334.
3. Haas, H. (2018). LiFi is a paradigm-shifting 5G technology. Rev. Phys. *3*, 26–31. https://doi.org/10.1016/j.revip.2017.10.001.
4. Jiang, B., Zhu, S., Ren, L., Shi, L., and Zhang, X. (2022). Simultaneous ultraviolet, visible, and near-infrared continuous-wave lasing in a rare-earth-doped microcavity. Adv. Photonics *4*, 1–8. https://doi.org/10.1117/1.AP.4.4.046003.
5. Karunatilaka, D., Zafar, F., Kalavally, V., and Parthiban, R. (2015). LED Based Indoor Visible Light Communications: State of the Art. IEEE Commun. Surv. Tutorials *17*, 1649–1678.
6. Zhao, Y., Long, M.J.C., Wang, Y., Zhang, S., and Aye, Y. (2018). Toward ultimate efficiency: progress and prospects on planar and 3D nanostructured nonpolar and semipolar InGaN light-emitting diodes. ACS Cent. Sci. *4*, 246–259. https://doi.org/10.1364/AOP.10.000246.
7. Zhang, J., Zhao, X., Shen, H., Lam, J.W.Y., Zhang, H., and Tang, B.Z. (2021). White-light emission from organic aggregates: a review. Adv. Photonics *4*, 1–17. https://doi.org/10.1117/1.AP.4.1.014001.
8. Xi, X., Zou, C.-L., Dong, C.-H., and Sun, X. (2022). Highly tunable broadband coherent wavelength conversion with a fiber-based optomechanical system. Adv. Photonics *4*, 1–9. https://doi.org/10.1117/1.AP.4.5.056003.
9. Shen, C., Lee, C., Ng, T.K., Nakamura, S., Speck, J.S., DenBaars, S.P., Alyamani, A.Y., El-Desouki, M.M., and Ooi, B.S. (2016). High-speed 405-nm superluminescent diode (SLD) with 807-MHz modulation bandwidth. Opt Express *24*, 20281–20286. https://doi.org/10.1364/OE.24.020281.
10. Dong, Z.Y., Lu, F., Ma, R., Wang, L., Zhang, C., Chen, G., Wang, A., and Zhao, B.; IEEE (2014). An Integrated Transmitter for LED-Based Visible Light Communication and Positioning System in A 180nm BCD Technology. In 2014 IEEE Bipolar/BiCMOS Circuits Technol. Meet., pp. 84–87.
11. Wei, L.Y., Hsu, C.W., Chow, C.W., and Yeh, C.H. (2018). 20.231 Gbit/s tricolor red/green/blue laser diode based bidirectional signal remodulation visible-light communication system. Photon. Res. *6*, 422–426. https://doi.org/10.1364/PRJ.6.000422.
12. Wang, W.C., Cheng, C.H., Wang, H.Y., and Lin, G.R. (2020). White-light color conversion with red/green/violet laser diodes and yellow light-emitting diode mixing for 34.8 Gbit/s visible lighting communication. Photon. Res. *8*, 1398–1408. https://doi.org/10.1364/PRJ.391431.
13. Li, X., Cheng, C., Zhang, C., Wei, Z., Wang, L., Fu, H.Y., and Yang, Y. (2022). Net 4 Gb/s underwater optical wireless communication system over 2 m using a single-pixel GaN-based blue mini-LED and linear equalization. Opt. Lett. *47*, 1976–1979. https://doi.org/10.1364/OL.452696.
14. TIAN, Z., Li, Q., Wang, X., Zhang, M., Su, X., Zhang, Y., Li, Y., Yun, F., and Lee, S.W.R. (2021). Phosphor-free micro-LEDs with ultrafast and broadband features for visible-light-communication. Photon. Res. *9*, 452–459. https://doi.org/10.1364/PRJ.413069.
15. Huang, W.-T., Peng, C.-Y., Chiang, H., Huang, Y.-M., Singh, K.J., Lee, W.-B., Chow, C.-W.,

Chen, S.-C., and Kuo, H.-C. (2022). Toward high-bandwidth yellow-green micro-LEDs utilizing nanoporous distributed Bragg reflectors for visible light communication. Photon. Res. *10*, 1810. https://doi.org/10.1364/PRJ.462519.

16. Quan, L.N., Quintero-Bermudez, R., Voznyy, O., Walters, G., Jain, A., Fan, J.Z., Zheng, X., Yang, Z., and Sargent, E.H. (2017). Highly Emissive Green Perovskite Nanocrystals in a Solid State Crystalline Matrix. Adv. Mater. *29*, 1605945. https://doi.org/10.1002/adma.201605945.
17. Zhang, J., Yang, Y., Deng, H., Farooq, U., Yang, X., Khan, J., Tang, J., and Song, H. (2017). High Quantum Yield Blue Emission from Lead-Free Inorganic Antimony Halide Perovskite Colloidal Quantum Dots. ACS Nano *11*, 9294–9302. https://doi.org/10.1021/acsnano.7b04683.
18. Kang, C.H., Dursun, I., Liu, G., Sinatra, L., Sun, X., Kong, M., Pan, J., Maity, P., Ooi, E.-N., Ng, T.K., et al. (2019). High-speed colour-converting photodetector with all-inorganic CsPbBr3 perovskite nanocrystals for ultraviolet light communication. Light Sci. Appl. *8*, 94. https://doi.org/10.1038/s41377-019-0204-4.
19. Song, J., Li, J., Li, X., Xu, L., Dong, Y., and Zeng, H. (2015). Quantum Dot Light-Emitting Diodes Based on Inorganic Perovskite Cesium Lead Halides (CsPbX3). Adv. Mater. *27*, 7162–7167. https://doi.org/10.1002/adma.201502567.
20. Tan, Z.-K., Moghaddam, R.S., Lai, M.L., Docampo, P., Higler, R., Deschler, F., Price, M., Sadhanala, A., Pazos, L.M., Credgington, D., et al. (2014). Bright light-emitting diodes based on organometal halide perovskite. Nat. Nanotechnol. *9*, 687–692. https://doi.org/10.1038/nnano.2014.149.
21. Fujieda, I., Kosugi, T., and Inaba, Y. (2009). Speckle noise evaluation and reduction of an edge-lit backlight system utilizing laser diodes and an optical fiber. J. Disp. Technol. *5*, 414–417. https://doi.org/10.1109/JDT.2009.2027612.
22. Wei, Y., Cheng, Z., and Lin, J. (2019). An overview on enhancing the stability of lead halide perovskite quantum dots and their applications in phosphor-converted LEDs. Chem. Soc. Rev. *48*, 310–350. https://doi.org/10.1039/C8CS00740C.
23. Zhao, S., Mo, Q., Wang, B., Cai, W., Li, R., and Zang, Z. (2022). Inorganic halide perovskites for lighting and visible light communication. Photon. Res. *10*, 1039. https://doi.org/10.1364/PRJ.450483.
24. Yu, B., Liang, S., Zhang, F., Li, Z., Liu, B., and Ding, X. (2021). Water-stable CsPbBr3 perovskite quantum-dot luminous fibers fabricated by centrifugal spinning for dual white light illumination and communication. Photon. Res. *9*, 1559–1568. https://doi.org/10.1364/PRJ.427066.
25. Dursun, I., Shen, C., Parida, M.R., Pan, J., Sarmah, S.P., Priante, D., Alyami, N., Liu, J., Saidaminov, M.I., Alias, M.S., et al. (2016). Perovskite Nanocrystals as a Color Converter for Visible Light Communication. ACS Photonics *3*, 1150–1156. https://doi.org/10.1021/acsphotonics.6b00187.
26. Liang, S., Lu, Z., Ding, X., Li, J., Tang, Y., Li, Z., and Yu, B. (2019). Perovskite liquid quantum dots as a color converter for LD-based white lighting system for visible light communication. In 2019 16th China International Forum on Solid State Lighting & 2019 International Forum on Wide Bandgap Semiconductors China (SSLChina: IFWS) (IEEE), pp. 277–279. https://doi.org/10.1109/SSLChinaIFWS49075.2019.9019760.
27. Chi, Y.-C., Hsieh, D.-H., Tsai, C.-T., Chen, H.-Y., Kuo, H.-C., and Lin, G.-R. (2015). 450-nm GaN laser diode enables high-speed visible light communication with 9-Gbps QAM-OFDM. Opt Express *23*, 13051–13059. https://doi.org/10.1364/OE.23.013051.
28. Wang, S., Zhu, T., Sabatini, R., Najarian, A.M., Imran, M., Zhao, R., Xia, P., Zeng, L., Hoogland, S., Seferos, D.S., and Sargent, E.H. (2022). Engineering Electro-Optic BaTiO 3 Nanocrystals via Efficient Doping. Adv. Mater. *34*, 2207261. https://doi.org/10.1002/adma.202207261.
29. Kumawat, N.K., Tress, W., and Gao, F. (2021). Mobile ions determine the luminescence yield of perovskite light-emitting diodes under pulsed operation. Nat. Commun. *12*, 4899. https://doi.org/10.1038/s41467-021-25016-5.
30. De Bastiani, M., Dell'Erba, G., Gandini, M., D'Innocenzo, V., Neutzner, S., Kandada, A.R.S., Grancini, G., Binda, M., Prato, M., Ball, J.M., et al. (2016). Ion Migration and the Role of Preconditioning Cycles in the Stabilization of the J - V Characteristics of Inverted Hybrid Perovskite Solar Cells. Adv. Energy Mater. *6*, 1501453. https://doi.org/10.1002/aenm.201501453.
31. Ferreira, D.L., and Alves, J.L.A. (2004). The effects of shape and size nonuniformity on the absorption spectrum of semiconductor quantum dots. Nanotechnology *15*, 975–981. https://doi.org/10.1088/0957-4484/15/8/019.
32. Rao, L., Sun, B., Liu, Y., Zhong, G., Wen, M., Zhang, J., Fu, T., Wang, S., Wang, F., and Niu, X. (2023). Highly Stable and Photoluminescent CsPbBr3/Cs4PbBr6 Composites for White-Light-Emitting Diodes and Visible Light Communication. Nanomaterials *13*, 355. https://doi.org/10.3390/nano13020355.
33. Jaque, D., and Vetrone, F. (2012). Luminescence nanothermometry. Nanoscale *4*, 4301–4326. https://doi.org/10.1039/c2nr30764b.
34. Osaki, H., Chou, C.M., Taki, M., Welke, K., Yokogawa, D., Irle, S., Sato, Y., Higashiyama, T., Saito, S., Fukazawa, A., and Yamaguchi, S. (2016). A Macrocyclic Fluorophore Dimer with Flexible Linkers: Bright Excimer Emission with a Long Fluorescence Lifetime. Angew. Chem., Int. Ed. Engl. *55*, 7131–7135. https://doi.org/10.1002/anie.201602239.
35. Dalfen, I., Dmitriev, R.I., Holst, G., Klimant, I., and Borisov, S.M. (2019). Background-Free Fluorescence-Decay-Time Sensing and Imaging of pH with Highly Photostable Diazaoxotriangulenium Dyes. Anal. Chem. *91*, 808–816. https://doi.org/10.1021/acs.analchem.8b02534.
36. Akkerman, Q.A., D'Innocenzo, V., Accornero, S., Scarpellini, A., Petrozza, A., Prato, M., and Manna, L. (2015). Tuning the optical properties of cesium lead halide perovskite nanocrystals by anion exchange reactions. J. Am. Chem. Soc. *137*, 10276–10281. https://doi.org/10.1021/jacs.5b05602.
37. Haque, A., Chonamada, T.D., Dey, A.B., and Santra, P.K. (2020). Insights into the interparticle mixing of CsPbBr 3 and CsPbI 3 nanocubes: halide ion migration and kinetics. Nanoscale *12*, 20840–20848. https://doi.org/10.1039/D0NR05771A.
38. D'Amico, A.A., and Morelli, M. (2022). Joint Frame Detection and Channel Parameter Estimation for OOK Free-Space Optical Communications. IEEE Trans. Commun. *70*, 4731–4744. https://doi.org/10.1109/TCOMM.2022.3177768.
39. Wei, Z., Wang, L., Liu, Z., Zhang, C., Chen, C.J., Wu, M.C., Yang, Y., Yu, C., Wang, L., and Fu, H.Y. (2022). Multigigabit Visible Light Communication Based on High-Bandwidth InGaN Quantum Dot Green Micro-LED. ACS Photonics *9*, 2354–2366. https://doi.org/10.1021/acsphotonics.2c00380.
40. Wang, Y.J., Gao, Y., Wang, L.N., Gao, X.M., and Hu, Z.F. (2022). Underwater Blue Light Communication Using Vertical-structure GaN Light Emitting Diode. J. Electron. Inf. Technol. *44*, 2703–2709. https://doi.org/10.11999/JEIT220328.
41. Clasen Hames, B., Sánchez Sánchez, R., Fakharuddin, A., and Mora-Seró, I. (2018). A Comparative Study of Light-Emitting Diodes Based on All-Inorganic Perovskite Nanoparticles (CsPbBr 3) Synthesized at Room Temperature and by a Hot-Injection Method. Chempluschem *83*, 294–299. https://doi.org/10.1002/cplu.201800014.
42. Mir, W.J., Alamoudi, A., Yin, J., Yorov, K.E., Maity, P., Naphade, R., Shao, B., Wang, J., Lintangpradipto, M.N., Nematulloev, S., et al. (2022). Lecithin Capping Ligands Enable Ultrastable Perovskite-Phase CsPbI 3 Quantum Dots for Rec. 2020 Bright-Red Light-Emitting Diodes. J. Am. Chem. Soc. *144*, 13302–13310. https://doi.org/10.1021/jacs.2c04637.
43. Swarnkar, A., Marshall, A.R., Sanehira, E.M., Chernomordik, B.D., Moore, D.T., Christians, J.A., Chakrabarti, T., and Luther, J.M. (2016). Quantum dot–induced phase stabilization of α-CsPbI 3 perovskite for high-efficiency photovoltaics. Science *354*, 92–95. https://doi.org/10.1126/science.aag2700.
44. Protesescu, L., Yakunin, S., Bodnarchuk, M.I., Krieg, F., Caputo, R., Hendon, C.H., Yang, R.X., Walsh, A., and Kovalenko, M.V. (2015). Nanocrystals of Cesium Lead Halide Perovskites (CsPbX 3 , X = Cl, Br, and I): Novel Optoelectronic Materials Showing Bright Emission with Wide Color Gamut. Nano Lett. *15*, 3692–3696. https://doi.org/10.1021/nl5048779.

STAR★METHODS

KEY RESOURCES TABLE

REAGENT or RESOURCE	SOURCE	IDENTIFIER
Chemicals, peptides, and recombinant proteins		
Lead(II) bromide, 99.999%, anhydrous, trace metals basis	J&K	10031-22-8
1-Octadecene, 90%, tech.	J&K	112-88-9
Oleic acid	aladdin	112-80-1
Oleylamine	aladdin	112-90-3
Lead iodide	aladdin	10101-63-0
Cesium carbonate, for synthesis,	J&K	534-17-8
Other		
Arbitrary waveform generator	RIGOL	DG70004
Oscilloscope	RIGOL	DS70504
Avalanche photodiode	Thorlab	APD210
Vector Network Analyzer	Keysight	E5061B
Universal Streak Camera	HAMAMATSU	C10910
PLQY	XIPUGUANGDIAN	XPQY-EQE-Adv

RESOURCE AVAILABILITY

Lead contact

Further inquiries and request for data, strains and resources should be directed to the lead contact Jingzhou Li lijingzhou@ucas.ac.cn.

Materials availability

This study did not generate new unique reagents.

Data and code availability

Data: All data reported in this paper will be shared by the lead contact upon request.
Code: This paper does not report original code.
Any additional information required to reanalyze the data reported in this paper is available from the lead contact upon request.

METHOD DETAILS

Preparation of $CsPbX_3$ (X = Br and I) perovskite QDs

$CsPbBr_3$ perovskite QDs were fabricated using the hot-injection method.[41–44] The precursor solution was prepared by the following synthesis method. The mixture composed of 7.5 mL of 1-Octadecene (ODE), 0.88 mL of oleic acid (OA), and 200 mg of $CsCO_3$ powder was prepared in a 25 mL three-neck flask and then stirred and degassed at 110°C for 1 hour under a nitrogen flow. It is important to note that the precursor solution, which can be stored for at least a month, should be heated to 110°C before use. Similar to the preparation method of the precursor, the reaction solution was synthesized by mixing 70 mg of $PbBr_2$ powder, 5 mL of ODE, 0.5 mL of OA, and 0.5 mL of oleylamine (OAM) into a three-necked flask, which was kept at 110°C under nitrogen and stirred for one hour. The mixed reaction solution was clear and free of powder. At this point, the injection begins. After the reaction solution was heated to 170°C, the precursor solution was injected into the reaction solution with a syringe. After 5 seconds of reaction, the three flask was cooled to room temperature by means of an ice water bath. Next, we started impurities, the solution was transferred to a 5 mL centrifuge tube by a pipette and centrifuged at 12100 revolutions per minute for 5 minutes to remove the supernatant, then added 2 mL toluene to the centrifuge tube, shook for one minute and centrifuged it again. At this time, the supernatant obtained was the $CsPbBr_3$ perovskite QDs with toluene as the solvent.

The method of synthesizing $CsPbI_3$ perovskite QDs is almost the same as that of synthesizing $CsPbBr_3$ perovskite QDs. The only difference was the using of 1.91×10^{-4} mol PbI_2 powder instead of $PbBr_2$ powder in synthesizing the reaction solution.

Preparation of the fluorescent film

We add 15 mL toluene and 3 g polymethyl methacrylate (PMMA) granules into a 30 mL glass bottle, then stir the mixture at 110°C for 1 hour until the granules are utterly dissolved. 200 μL solution of the prepared $CsPbBr_3$ perovskite QDs solution was injected into the PMMA solution and stirred for 30 min. With the using of a pipette gun, five microliters of the mixed solution were placed on the quartz glass sheet. After 5 minutes of evaporation, the fluorescent film was formed.